IMPROVEMENT OF WELDABILITY OF DISSYMETRIC ASSEMBLY WITH VERY THIN SHEET DURING RESISTANCE SPOT WELDING

J. QUEVAL*, E. GESLAIN*, P. ROGEON*, T. PIERRE*,
C. POUVREAU*, L. CRETTEUR**, S. MARIE***

**Université Bretagne Sud, IRDL, CNRS FRE 3744, Lorient, France*
*** ArcelorMittal Global R&D, Montataire, France*
**** Transvalor S.A., Mougins, France*

ABSTRACT

In automotive industry, to simultaneously impact safety and light weighting for reducing energy consumption, new families of high strength steel have been introduced in the design of body in white. Some combinations of dissimilar sheets, including a very thin sheet, cause weldability problems and difficulties to the optimization of the process parameters setting. Thanks to the progress achieved in numerical and computer engineering fields, modelling and numerical simulation is a relevant approach, to understand the difficulties encountered during resistance spot welding of these assemblies, and to search solutions to improve the weldability. This work aims at the improvement of the weldability of a dissymmetric combination of three dissimilar sheets: a very thin (0.57 mm) zinc coated low carbon steel sheet, a thick (1.47 mm) zinc coated advanced high strength steel sheet, and a thick (1.2 mm) aluminum-silicon coated press hardened sheet.
A numerical axisymmetric 2D Electro-Thermo-Mechanical model developed with the software FORGE® is used to improve the knowledge about the mechanisms which influence the nugget formation and growth, and its penetration inside the cover thin sheet. Experimental evolutions of thermal and electrical contact resistances evolutions, at electrode/sheet and sheet/sheet interfaces, strongly dependent of coatings properties, are embedded in the model and considered dependent on contact temperature and normal stress. The contact radius evolutions, involving the normal contact stresses and the current density distributions in the assembly, are calculated during squeezing, welding, and forging stages.
The model is consistent with several experimental observations (nugget size, contact radii, dynamic resistance) issued from welding tests. Thanks to this model, the important effect of the interfacial mechanisms on the formation and the growth of the molten pool have been highlighted. Furthermore, the influence of the process parameters (current, force) and of the curvature radius of the rounded tip electrodes on the penetration of the welding pool into the thin sheet have been investigated.

Keywords: Resistance spot welding, interface, numerical modeling, contact resistance, physics coupling

INTRODUCTION

In automotive industry, lightweighting of automobiles is one of the principal engine for innovation for reducing the energy consumption. ArcelorMittal, the world leader in the

production of steel works to develop new steels, more resistant in order ensure the security inside the vehicle and meet the same specifications with thinner steel sheets.

A body in white is composed by different grade of steels and their position depends on their mechanical properties, duties. In some part of the body in white, it can be necessary to assemble three dissimilar sheets by resistance spot welding (RSW). These combinations create very dissymmetric assemblies that raise problems of weldability with difficulties to grip the thin sheet with the two others, as mentioned by Nielsen [1] or by Kaars [2]. In the case of this study, the assembly is made by:

- a zinc coated low carbon steel sheet (AM54 – 0.6 mm in depth)
- a zinc coated high strength steel (HSS) sheet (DP600 – 1.5 mm in depth)
- an Aluminum-Silicon (Al-Si) coated press hardened steel (PHS) sheet (Usibor – 1.2 mm in depth).

The purpose of this study is to understand the source of the difficulties met during the RSW of this assembly. It is about the identification of the parameters that influence the formation and the development of the molten pool and the penetration of the nugget in the thin sheet. Solutions to improve the grip of the thin sheet could be given. This study is realized through a numerical approach using the software Forge®. A specific attention is given to the interfacial phenomena.

First, the model is validated, comparing numerical and experimental results obtained from welding tests [3]. Than, it is used here mainly to highlight the main mechanisms which influence the formation and the development of the nugget inside the dissymetric assembly.

NUMERICAL MODEL

GEOMETRY AND MESH

Rounded tip electrodes (type A0-13-18-32) with diameter 13 mm and curvature radius 32 mm have been designed. Due to the revolution geometry of the electrodes, the geometry of the model can be assumed 2D-axisymetric. The coatings of the sheets are taken into account through interfacial properties in the contact conditions, and so they are not integrated in the geometry. $e_1 = 0.54$ mm, $e_2 = 1.45$ mm, and $e_3 = 1.14$ mm are respectively the thickness values of the sheets AM54, DP600 and Usibor respectively.

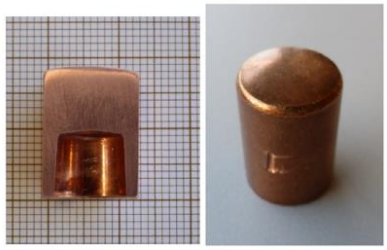

Fig.1 Reference electrodes type A0-13-18-32 – diameter 13mm, curvature radius 32mm

The initial mesh of the assembly (Fig.2) is achieved by using linear triangular elements. The size of an element is defined by the average length of its edges. At the proximity of the contact zones, the average size is 0.1 mm. In the zones where the variation of the physical phenomena and the gradients should be high, average size is 0.25mm. Elsewhere the average size is 0.4 mm.

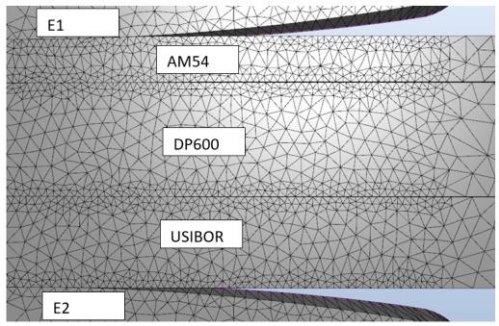

Fig.2 Initial mesh of the assembly

The criterion for activating the remeshing is automatic and is based on the increasing of the deformation between two remeshing operations. The remeshing is activated after a maximum deformation of 100 %.

GOVERNING EQUATIONS

Based on some similar recent numerical works ([4], [5], [6]), the model developed here takes into account the main phenomena involved in the process (electric, thermic, mechanic) with their coupling occurring inside the material and along the interfaces. The metallurgical transformations in the steels are not explicitly taken into consideration in this model. Only the austenitic transformation during heating is implicitly taken into consideration in the evolution of the physical properties and mechanical behavior with the temperature. The transformations during the cooling are not correctly modeled, but their effect concern, principally, the residual

stresses [7], which are not in the focus of this study. The effect of the magneto-hydro-dynamic (MHD) phenomenon that are susceptible to occur inside the molten nugget are supposed negligible and are not taken into consideration, according to Wan [6], Wang [5], or Raoelison [4], but in contradiction with Wei ([8], [9]) or Li [10]. However, in the MHD model developed by Wei ([9], [8]) the contact radii are assumed constant. This numerical approach is not suitable in our configuration were convex tip electrodes promote indentation inside the sheets and will induce the increase of the contact radii as a consequence.

The electrical problem consists of solving the equation of electrical current conservation in stationary condition:

$$div(\vec{J}) = 0 \qquad (1)$$

With J (A/m²) the current density. According to Ohm's law:

$$div(\ \sigma^{el}(T)\overrightarrow{grad(V)} = 0 \qquad (2)$$

With V (Volt) the electrical potential and $\sigma^{el}(T)(\Omega.m)^{-1}$ the electrical conductivity. The evolutions of the electrical conductivity of the different steels and copper alloy (CuCrZr) of the electrodes come from previous work [3], [11] and [12].

The governing equation for the transient thermal analysis is given by the energy balance :

$$\rho^{vol}\frac{\partial H(T)}{\partial t} = div(\ \lambda(T)\overrightarrow{grad}(\mathrm{T})) + Q \qquad (3)$$

Equation in which one, the heat generation by Joule effect is expressed as follows :

$$Q = \overrightarrow{grad^{T}}(V)\sigma^{el}(T)\overrightarrow{grad}(V) \qquad (4)$$

Where T(K), ρ^{vol} $(kg.m^{-3})$, H $(J.kg^{-1})$, $\lambda(W.m^{-1}.K^{-1})$, et Q $(W.m^{-3})$ denotes respectively the temperature, the mass per unit of volume, the enthalpy per unit of mass and the internal heat generation by Joule effect. The thermophysical properties of the steels and CuCrZr alloy come from previous work [3], [11] and [12].

The mechanical analysis consists in solving the equilibrium equation :

$$div(\vec{\sigma}) = -\rho f \qquad (5)$$

With σ the stress tensor, ρ the mass density and f the force.

During the welding, the temperatures inside the sheets vary in a large range of temperature, from the ambient temperature to high temperatures higher than the liquidus temperature (1535°C). To calculate the strains, a good description of the behaviors of the material at high temperature is needed [7]. Near the melting temperature, sheets become sensitive to the strain rate. The description of the viscoplastic behavior of steels has been input in data tables. The

work-hardening curves at different strain rates from 10^{-3} to 10^{3} s^{-1} and at different temperatures from 20 °C to 1600 °C are given for each steel. The material data for the sheets are given by the software JMatPro® which allows the calculation of the thermophysical and mechanical properties of the steels from their chemical composition. For CuCrZr alloy, plastic behavior has been assumed [11].

The tensor of the strain rates can be decomposed into a reversible part corresponding to the thermoelastic strains and an irreversible part corresponding to viscoplastic strains.

$$\dot{\epsilon} = \dot{\epsilon_{\text{rev}}} + \dot{\epsilon_{vp}} = \dot{\epsilon_{th}} + \dot{\epsilon_{el}} + \dot{\epsilon_{vp}} \quad (6)$$

The equivalent load stress σ_{eq} (6), for dense materials only depends on the second invariant J_2 (8) of the stress deviator tensor:

$$\sigma_{eq} = \sqrt{\frac{3}{2} J_2} \quad (7)$$

$$J_2 = \frac{1}{2} s^2 = \frac{1}{2} tr(s.s) \quad (8)$$

$$s = \sigma - \frac{1}{3} tr(\sigma) I \quad (9)$$

The criterion of plasticity fc permit to define the domain of the stress space within which one all the deformations generated are elastic deformations (reversible). In the case of the viscoplasticity with a threshold σ_y and isotropic hardening R, it corresponds to the von Mises criterion:

$$fc = \sigma_{eq} - (\sigma_y + R) \quad (10)$$

BOUNDARY CONDITIONS

Specific boundary conditions are applied during each stage, squeezing, welding, and forging (Fig.3):

- During squeezing, welding, and forging a mechanical load (F=4000 N) is applied on the upper electrode,
- During welding, electric current is imposed on upper electrode (I=8500 A), and mass (V= 0) on the lower electrode.
- During welding and forging, water convective exchanges are imposed inside the electrode holes, and air radiative and convective exchanges are imposed on the surfaces of the sheets and electrodes.

The process parameters values are those used during the experimental test taken as reference for this study [3].

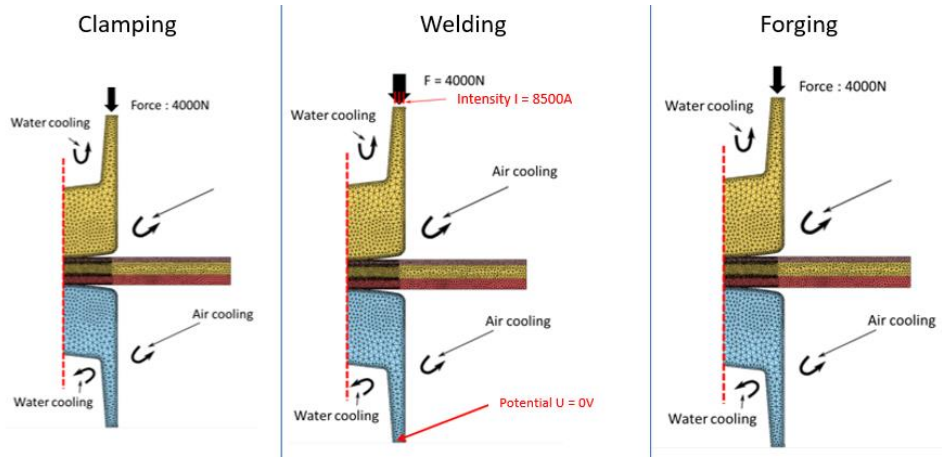

Fig.3 Boundary conditions applied on the model corresponding to the welding conditions

CONTACT CONDITIONS

Due to their curvature radius, electrode tips indent inside the sheets during welding stage. Furthermore, important thermal dilatation of sheets occurs, due to the high temperature reached inside the assembly. Consequently, contact conditions change at macroscopic scale.

In fact, the apparent electrode/sheet (E/S) contact area increases during the welding time, and the current density in the assembly and the contact pressure at the interfaces decreases, as a consequence. For the mechanical contact modelling, sliding conditions are assumed for the whole E/S and sheet/sheet (S/S) interfaces.

At the microscopic scale, due to the imperfections of the contact surfaces (surface roughness, chemical pollutants), the interfaces are not perfect and a contact resistance opposes to the current and heat flow. The electrical and thermal contact resistances at E/S and S/S interfaces are taken into account through 3 contact parameters (RCE, RCT, α) [12]. The electro-thermal contact conditions are considered purely resistive. The power generation by Joule Effect ϕ inside the RCE, crossed by the current density J, ($\phi = RCE.J^2$ (W/m^2)), is spread over the two surfaces in contact, thanks to a partition coefficient (α) imposed to 0.5 outside the thermal contact resistance RCT ([13], [14]).

MATERIALS DATA

The differences between physical and mechanical properties of the sheets contribute strongly to the dissymmetry of the studied assembly (Table.1, Fig.4). For example, higher resistivity and lower solidus temperature for the two thicker sheets will promote the efficiency of the Joule heating and the earlier initiation of nugget inside USIBOR and DP600, respectively. Furthermore, the lower mechanical resistance of the thin sheet AM54 will enhance the

indentation of the rounded tip electrode during the welding stage with the decrease of the current density and then of the Joule heating inside the thin sheet as a consequence.

Table.1 Thermo-physical and mechanical properties of the sheets at ambient temperature (293°K)

	Thermo-physical properties at 293°K				Melting temperature	Mechanical properties at 293°K	
Nom	Density ($kg.m^{-3}$)	Heat capacity ($J.kg^{-1}.K^{-1}$)	Thermal conductivity ($W.m^{-1}.K^{-1}$)	Electrical resistivity ($\mu\Omega.m$)	$T_{solidus}$ (°C)	Re (MPa)	Rm (MPa)
AM54	7750	446	66.1	0.12	1531	180	315
DP600	7790	447	42.2	0.27	1480	383	626
Usibor	7940	452	38.6	0.24	1456	1100	1500

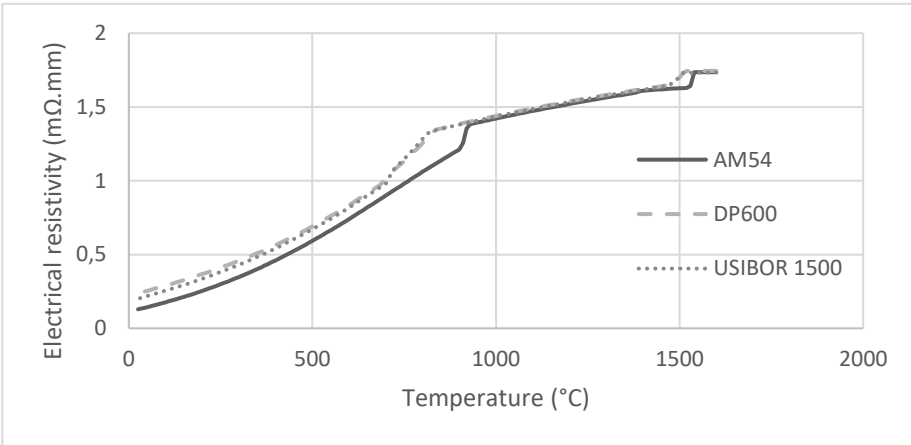

Fig.4 Electrical resistivity evolutions of the steel sheets

In several RSW numerical models [9], [5], [15], the RCE are calculated through correlations or phenomenological laws and the RCT are issued from the RCE by using Wiedmann-Franz law. On the contrary, in this model, concerning the interfacial properties for the E/S and S/S contacts, the evolution of the thermal and electrical contact resistances, RCT and RCE, have been characterized on a specific device [16] in function of the pressure and the temperature (Fig.5, Fig.6). Due to the plastic deformations of the asperities, the evolution of the RCE and RCT are irreversible in function of the pressure and the temperature. The bulk resistances of the coatings are directly embedded in the values of the contact resistances. Due to the specific properties of the Al-Si coating (lower conductivity, higher hardness and roughness) comparatively to the zinc coating, the contact resistances (RCE(3), RCE(4)) for the two interfaces with the Usibor sheet are huger (Fig.5, Fig.7). In this study, the contact resistances are implemented in the numerical model but their irreversibility in function of the temperature and the pressure is not yet taken into consideration.

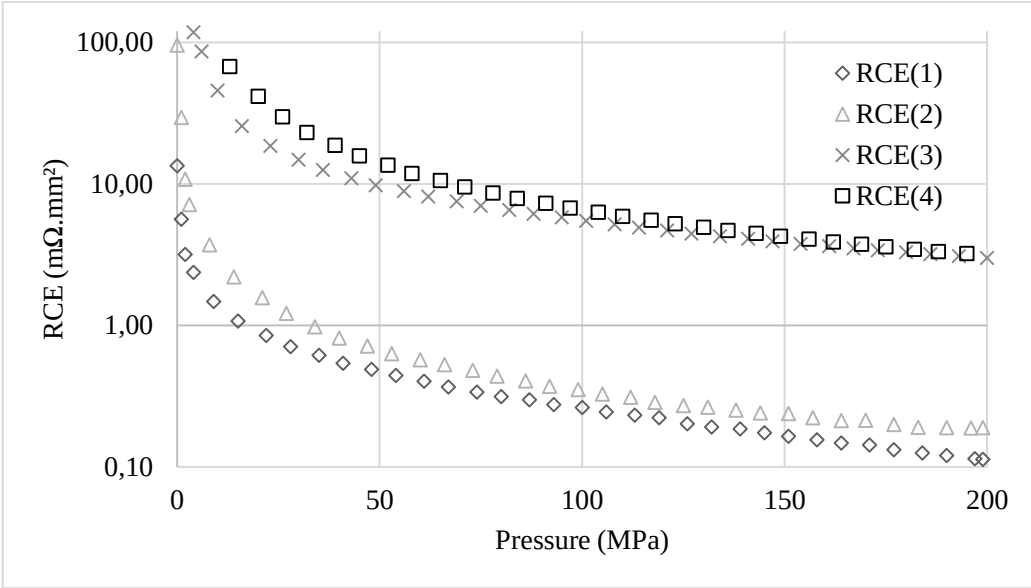

Fig.5 Experimental evolutions of the RCE for each interface versus the contact pressure P at ambient temperature) (1: CU_AM, 2: AM_DP, 3: DP_USI, 4: USI_CU)

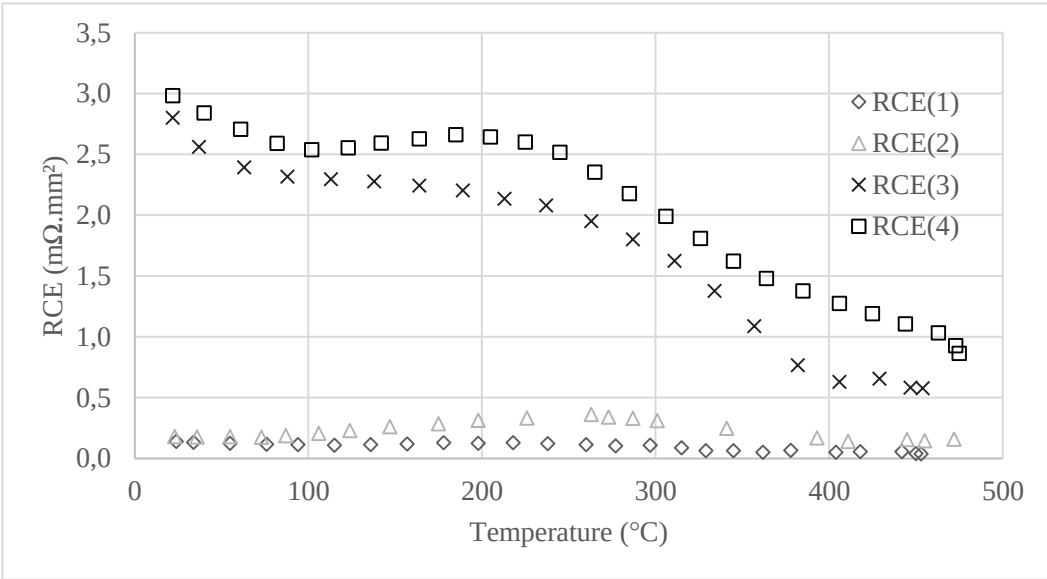

Fig.6 Experimental evolutions of the RCE for each interface versus the temperature at 200MPa (1: CU_AM, 2: AM_DP, 3: DP_USI, 4: USI_CU)

RESULTS AND ANALYSIS

VOLTAGE BETWEEN THE ELECTRODES

The evolutions of the numerical and experimental upper electrode voltage are really in good accordance until 40 ms (Fig.7). Just after 40 ms the numerical curves present a jump of the potential not observed experimentally. After 150 ms the numerical and experimental curves are in good accordance again.

The voltage depends on the electric current evolution imposed (Fig.7) and on the dynamic electrical resistance of the assembly which varies with the electrical contact resistances, the electrical resistivity of the sheets, the thickness of the sheets, and with the contact radii. The pic of tension is obtained after that the welding intensity reaches its maximal value on the plateau (Fig.7).

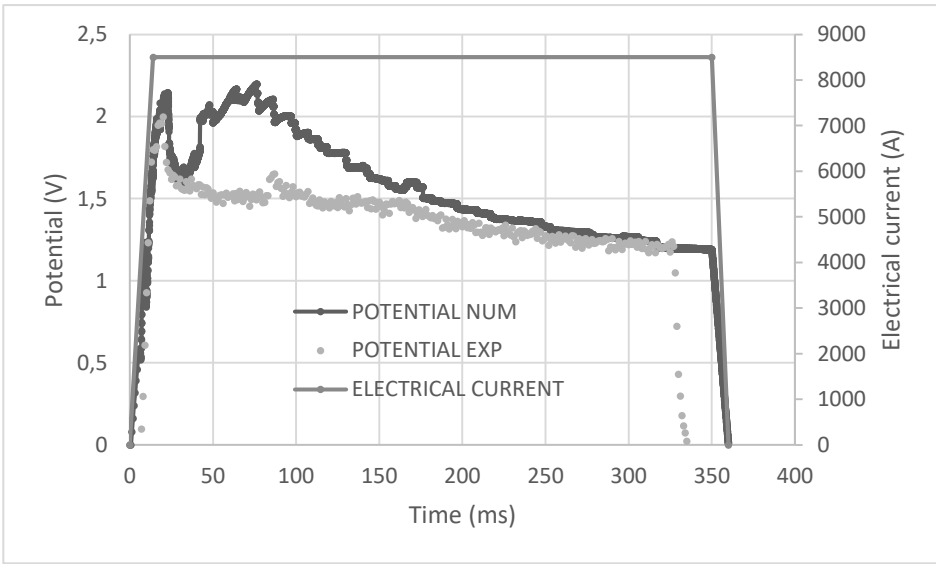

Fig.7 Numerical and experimental potential measured

STRAINS OF THE ASSEMBLY, CONTACT RADII AND THICKNESS

At the end of the clamping stage, the experimental contact radii measured with pressure-sensitive paper Prescale® are 0.5 mm appear higher than the numerical values (Fig.8). The measurement technique with ink-laden microbeads may overestimate the values of the radii [3] and explains the observed discrepancies. During the welding stage, at the interface

electrode/thin sheet (CU_AM), the evolution of the measured and calculated radii intersects around 80ms, then diverge after (Fig.8). The numerical radii calculated are higher than the experimental radii measured. For the interface Usibor/electrode (USI_CU), the calculated values of the contact radii are lower than the experimental ones on the whole welding time (Fig.8). Despite the differences, the dynamic of the evolutions of the E/S contact radii obtained by the numerical model are rather similar to values issue from experimental tests.

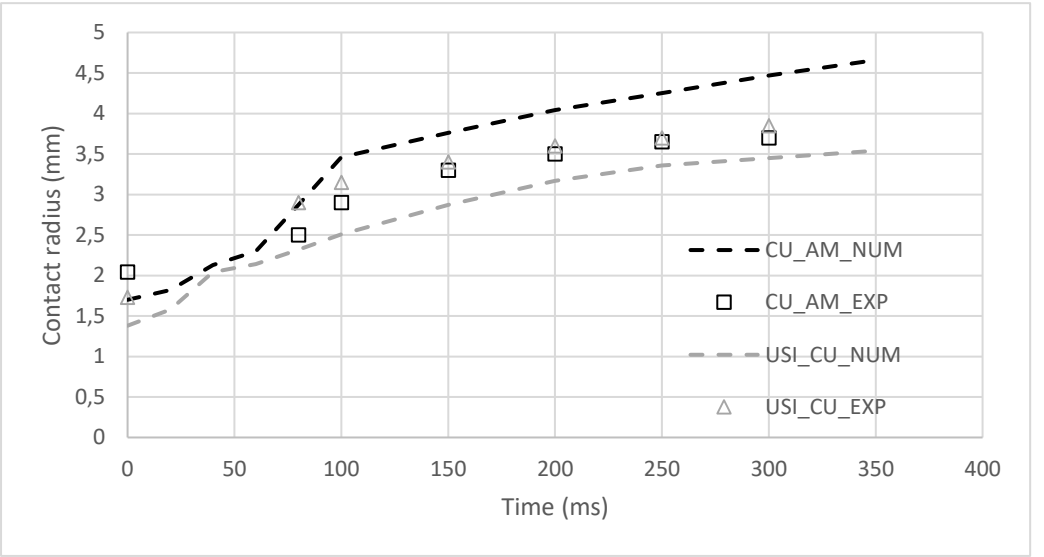

Fig.8 Comparison between numerical and experimental contact radii evolutions for the two E/S interfaces

The assembly of three sheets also meets a variation of its thickness e ($e = e_1 + e_2 + e_3$) during the process. Two antagonist forces are responsible of this variation:

- The squeezing force applied by the electrodes which induces the indentation of the rounded tip electrodes inside the sheets
- The thermal dilatation of the materials

The thickness increases during the first part of the welding step ($0 \rightarrow 190\ ms$) (Fig.9), due to the important temperature rise in the assembly. During this period of time the heat production by Joule effect is largely higher than the thermal losses, because of the electrical contact resistance effects and because of the small contact areas which induce high current density values in the assembly. The indentation of the electrode tips inside the sheets begins, but the evolution of the thickness is mostly driven by the thermal dilatation. The molten pool size also increases quickly in thickness until around 200 ms (Fig.13).

For a time greater than 190 ms the thickness of the assembly decreases. Indentation of electrode tips inside the sheets become the prevalent factor, due to the softening of the sheets with the strong heating in the first moment.

When the welding current is interrupted after 350 ms, the thickness decreases continuously, mainly due to the thermal shrinkage, during the forging stage till 860 ms and during the air cooling stage (duration of the cooling stage : 120s).

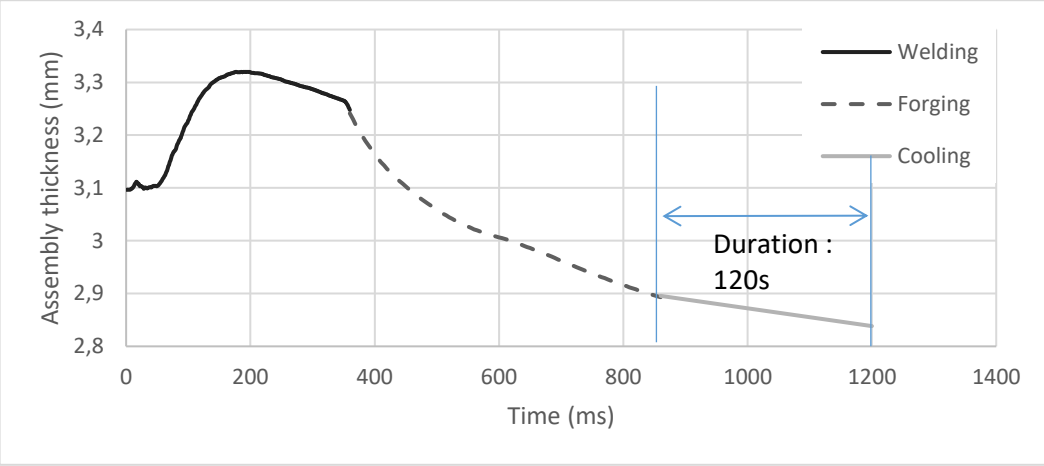

Fig.9 Evolution of the assembly thickness

RADIUS AND THICKNESS OF THE MOLTEN POOL, PENETRATION IN THE THIN SHEET

The numerical shapes of the molten pool appear in good accordance with experimental ones for different interrupted times 80 ms, 150 ms, 300 ms (Fig.10). However, the sizes cannot be compared directly. The numerical molten pool sizes are obtained when the fusion zone meets high temperatures (2800-3000°C) and high dilatation rate. In the second case, the experimental solidified nugget is obtained after thermal shrinkage at ambient temperature. Only the experimental and numerical localization and dynamic evolution of the nugget can be compared.

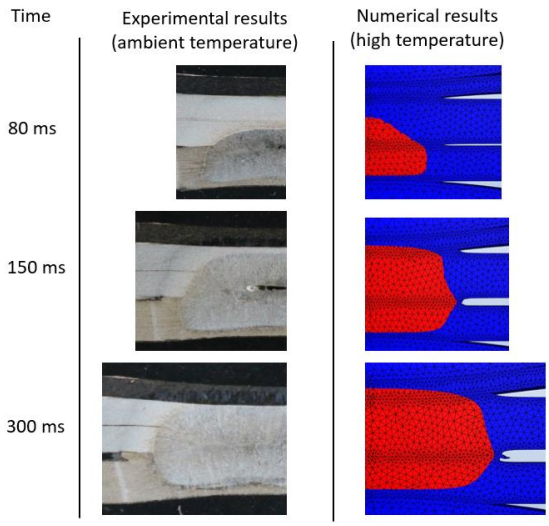

Fig.10 Comparison of the localization and the shape of the numerical molten pool (high temperature) and the experimental nugget (ambient temperature)

The calculations show that the molten nugget appears inside the Usibor plate around 40 ms (Fig.11) at the opposite of the thin sheet. After it develops quickly in thickness inside the DP600 and towards the AM54 thin sheet (Fig.11). The origin is linked to the huge contact resistances at interfaces with the Usibor sheet which initiate overheating at these interfaces and locate the hot spot within the Usibor sheet (Fig.19).

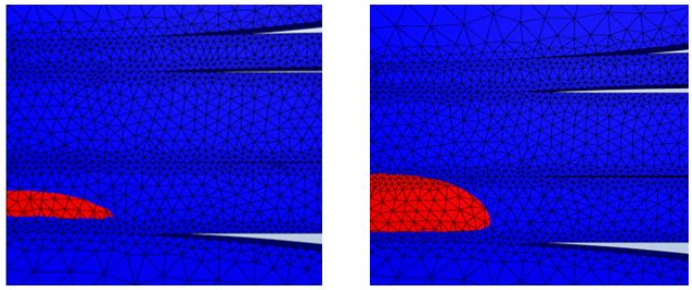

Fig.11 Localization and shape of the molten pool at 40ms and 60ms

In this section, the numerical and experimental dimensions of the nugget are compared more precisely (thickness e_N, radii (r_{N1} r_{N2}), penetration in the thin sheet p) (Fig.12).

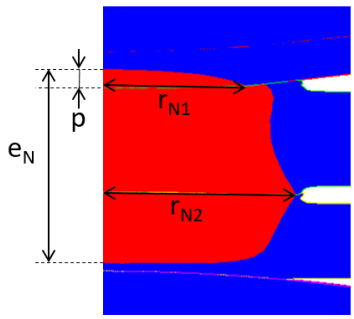

Fig.12 Dimensions of the nugget: e_N (thickness), r_{N2} (radius at the interface USI_DP), r_{N1} (radius at the interface AM_DP), p (penetration inside the thin sheet).

The numerical and experimental evolutions of the thickness of the molten pool present similar dynamics (Fig.13). The thickness increases quickly, then meets a maximum around 200 ms, and decreases slowly until the electrical current is cut off at the end of the welding at 350 ms. The numerical values, taking into account the strong thermal dilatation of the molten pool, are logically higher than the experimental values measured at ambient temperature after cooling of the assembly. The numerical thickness values obtained after forging stage from 3 interrupted points (80 ms, 150 ms, 300 ms) are logically nearer (Fig.13).

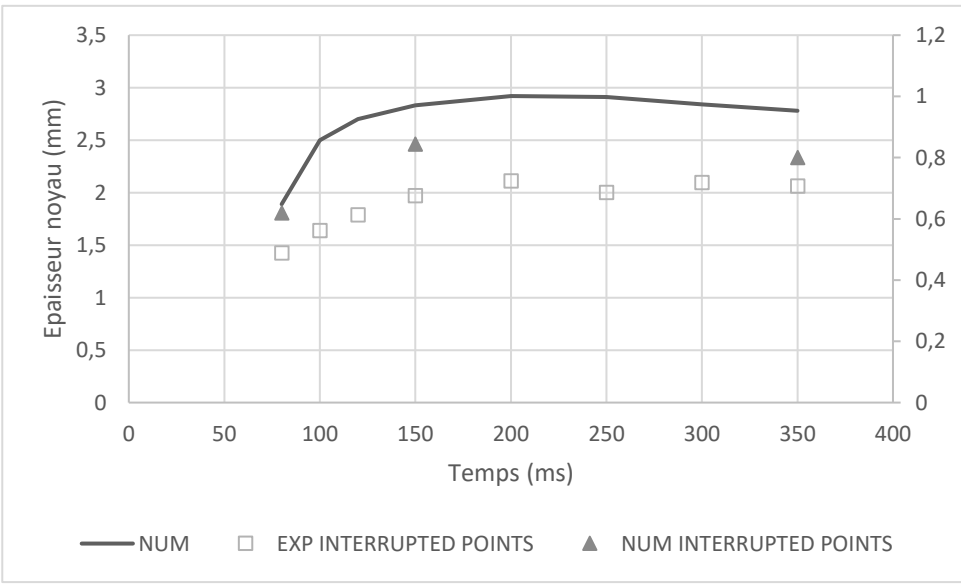

Fig.13 Evolution of the depth of the molten pool (during the welding) and the nugget (after cooling)

The thickness evolution of the molten pool is driven by the equilibrium between the heating by Joule effect, at the interfaces ($RCE.J^2$ (W/m^2)) and inside the sheets ($1/\sigma.J^2$ (W/m^3)), and

the heat losses mainly by conduction through the electrodes. Indeed, until the values of the contact radii (Fig.8) remain sufficiently low, heating is dominant and the nugget thickness increases quickly. After 200 ms when the contact radii reach high values with the indentation of the electrode tips inside the sheets, the current density drops causing a decrease of the power heating and the heat losses increase and become prevalent. Consequently, the nugget thickness regresses slightly.

Furthermore, the evolutions of the numerical and experimental nugget r_{N2} are in pretty good adequacy (Fig.14), by taken into consideration the preceding remarks on the potential causes of distortions.

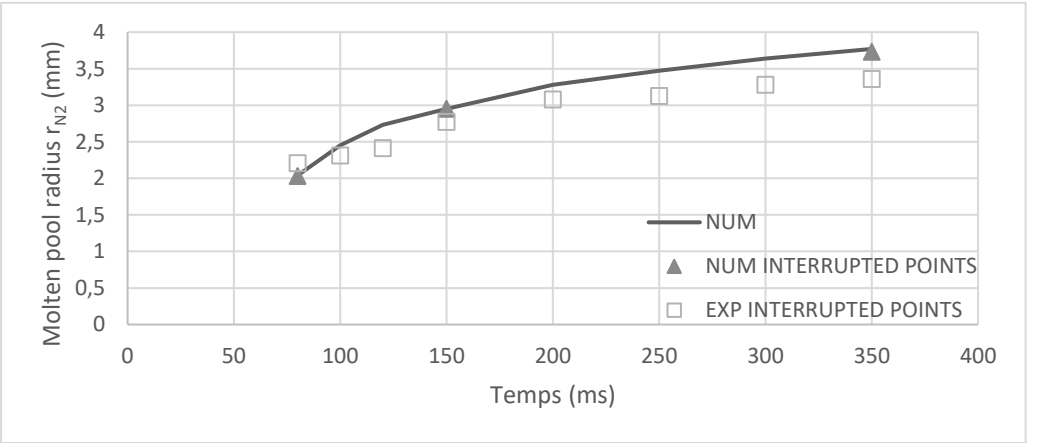

Fig.14 Comparison between experimental nugget radius and numerical molten pool radius during welding stage

The penetration of the molten pool inside the AM sheet reaches a maximal value 0.34 mm at 200 ms (Fig.15) and decreases slightly after. The experimental value 0.14 mm measured after the end of the cooling stage is significantly lower, which indicates that the numerical molten pool thickness is certainly overestimated. The radius rN1 of the molten pool at the contact CU_AM increases continuously during the welding stage and reaches 3 mm.

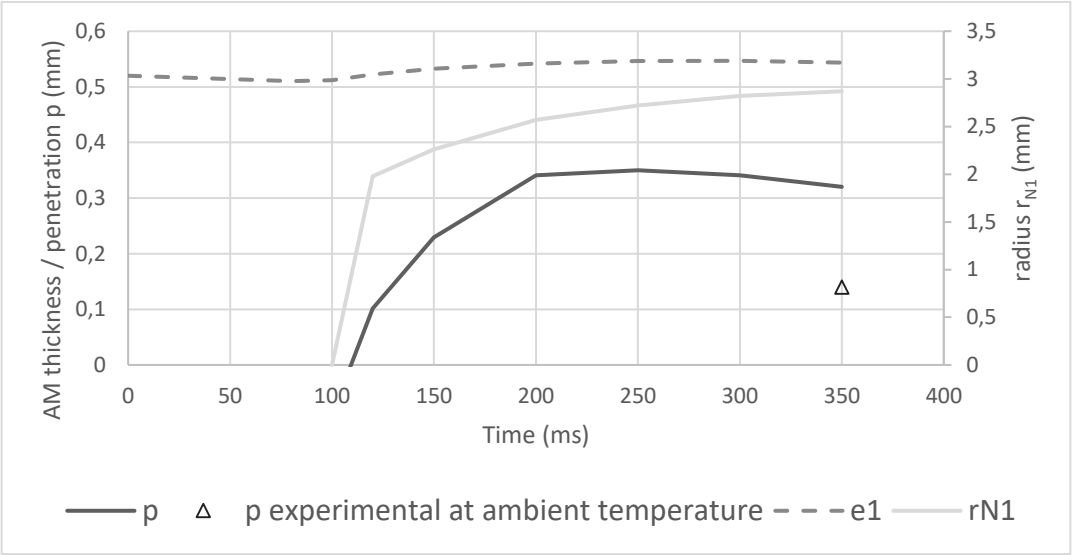

Fig.15 Penetration of the molten pool inside the AM sheet

ELECTRO-THERMO-MECHANICAL COUPLING PHENOMENA AT CONTACTS

The normal stress at the different interfaces present different initial values and vary strongly in function of the time (Fig.16), with the indentation of the electrode tips inside the sheets. The maximal values of the normal stress are calculated after the squeezing stage. When the indentation increases, a drop of the normal stress is observed, and the evolutions at the different interfaces become similar. The drop is particularly important for the USI_CU contact. After t = 60 ms, the normal stresses at each contact are similar and continue to decrease slowly during the welding.

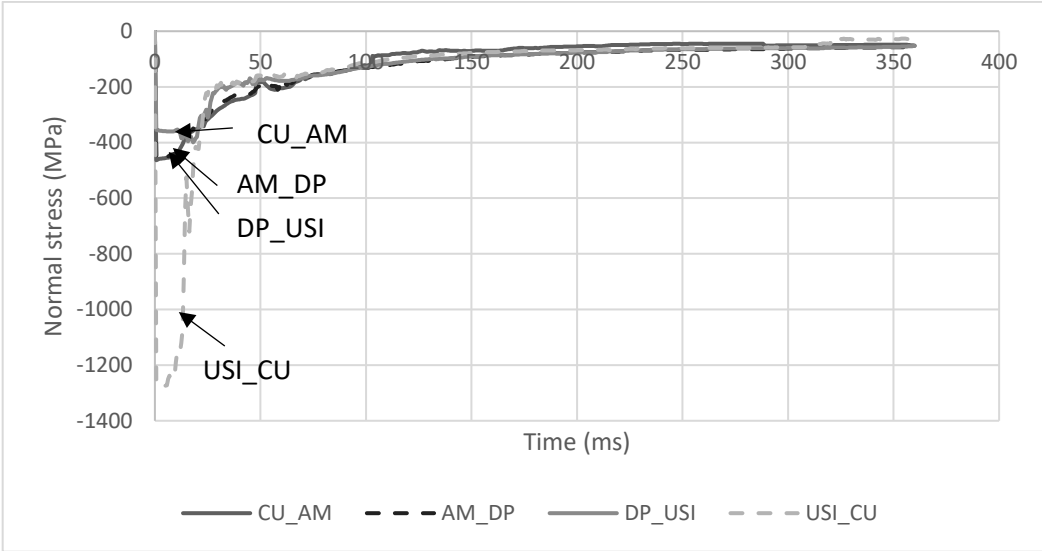

Fig.16 Normal stress calculated along the contact radii in function of the time

Furthermore, the distributions of the normal stress are not uniform, and the values are higher at the extremity of the contact zone (-400 MPa) versus (-160 MPa) along the contact axis (Fig.17).

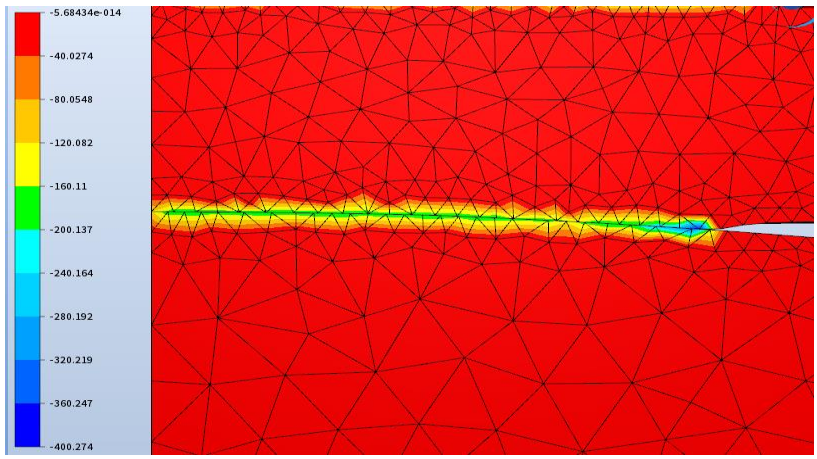

Fig.17 Evolution of the normal stress along the contact USI_CU at a time t

The axisymmetric geometry of the electrodes provides a non-uniform current density distribution on the contact zones, with a peak at the extremity of the contact zones (Fig.18).

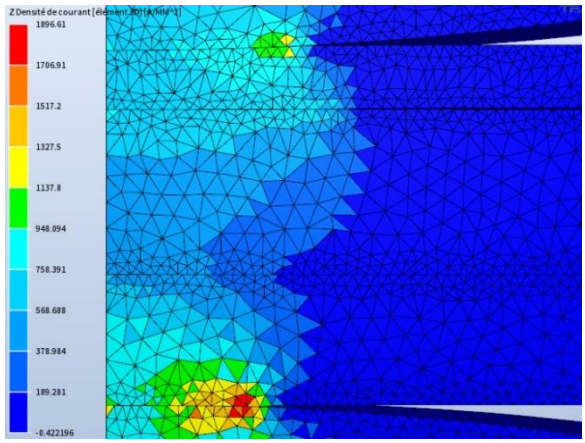

Fig.18 Repartition of the current density along the interfaces (J (A/mm^2))

The non-uniform distribution of the current density (Fig.18) provides non-uniform power heating and non-uniform temperature distribution as a consequence (Fig.19 and Fig.22). At the first moment of the welding stage, a peak of temperature is calculated at the periphery of the Electrode/Usibor contact zone, in good adequacy with observations by infrared camera [3] (Fig.19).

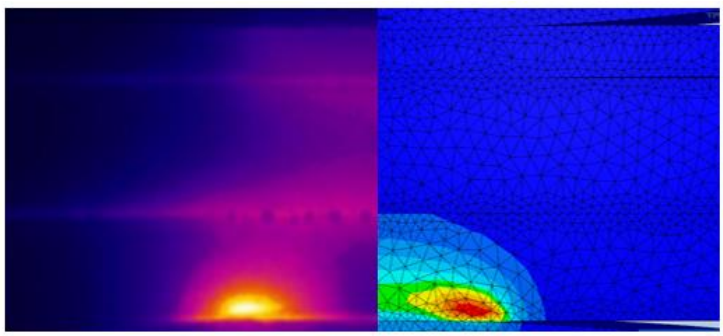

Fig.19 Peak temperature at the periphery of CU_USI interface in the first moments

With the non-uniformity of the contact pressure and of the contact temperature along the interface, the values of the contact resistances RCE and RCT are also non-uniform and are lower at the periphery of the contact zones where the contact temperature and the normal-stresses are the highest. In the model, the contact resistances RCE and RCT could artificially increase when the contact temperature or the normal stress decrease. This is the case at the interface between the Usibor sheet and the lower electrode, where the electrical contact resistance increases with the drop of the normal stress at this interface (Fig.20), while the contact temperature remains relatively low and inferior to the melting point of the Al-Si

coating (around 1000 °C) (Fig.22). This phenomenon is not observable at the interface DP_USI (Fig.21) because the contact temperature increases quickly over the melting temperature of the Al-Si coating.

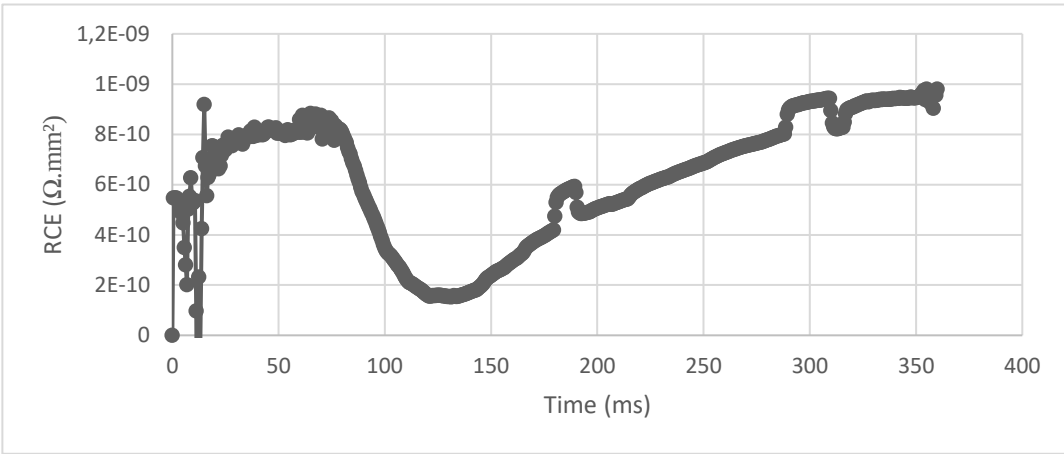

Fig.20 Electrical contact resistance at the interface USI-CU

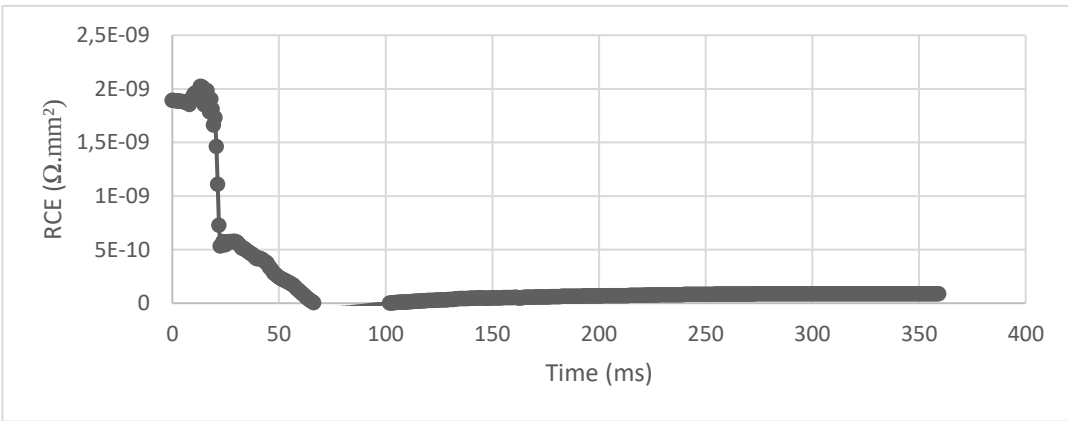

Fig.21 Electrical contact resistance at the interface DP-USI

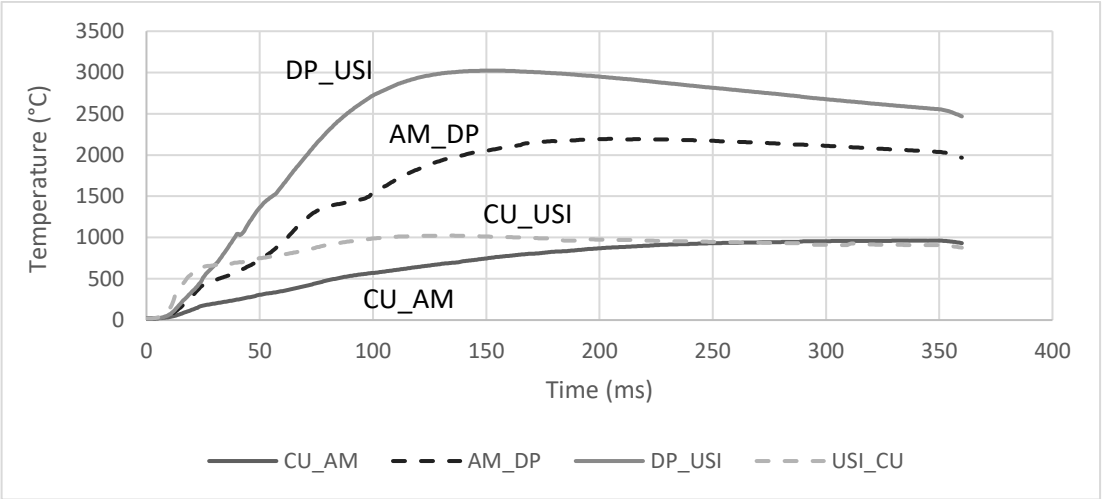

Fig.22 Contact temperature calculated at E/S and S/S contacts

The values of the RCE(P,T) at Usibor/Electrode interfaces increase in the model between 30 ms and 80 ms (Fig.20), because of the reversible contact conditions assumed in the model. In fact, when the contact radii increase the contact pressure decreases and the numerical RCE values increase. On the contrary, at the DP_USI interface, the RCE decrease (Fig.21), despite the decrease of the contact pressure, because the temperature rise is largely higher at this interface (Fig.22). The artificial increase of the RCE(P,T) at the interface Usibor/Electrode could probably explain the abnormal overheating obtained numerically in the assembly (Fig.10), and the jump observed on the numerical voltage evolution (Fig.7).

CONCLUSION

In this study, achieved in partnership with ArcelorMittal, a numerical model has been developed using the software Forge® to simulate the resistance spot welding of a 3 dissimilar sheets assembly, including a very thin sheet. The aim is to give a better understanding of the difficulties encountered to succeed the weldability of the thin sheet.

The good adequacy found between numerical and experimental results, concerning the E/S contact radii, the size of the nugget with the penetration inside the thin sheet and the voltage between electrodes, proves the reliability of the model and the suitability of the software Forge® to simulate the RSW process. The huge electrical and thermal contact resistances at the two interfaces with the Usibor sheet, because of the Al-Si coating, promote the initiation of the nugget inside this sheet, far from the thin sheet. The growing of the nugget in thickness and the penetration inside the thin sheet appear in the first moment of the welding stage, till the contact radii become too important with indentation of rounded tip electrodes inside the

sheets. After the nugget progresses only in diameter at the two S/S interfaces till the end of welding stage.

Due to the complex spatio-temporal contact conditions, with the non-uniform distributions of the normal-stress, of the current density, and of the contact temperature, a great attention should be paid to the modelling of the contact conditions. To improve the numerical model, irreversibility laws for the contact resistances should be imbedded and optimization of the extrapolation of the mechanical behavior laws at high temperature for the steels could be assessed.

References

[1] C. V. NIELSEN, K. S. FRIIS, W. ZHANG, N. BAY: 'Three-Sheet Spot Welding of Advanced High-Strength Steels', *Welding Journal 90*, pp. 32s-40s, 2011.

[2] J. KAARS, P. MAYR, K. KOPPE: 'Simple transition resistance model for spot welding simulation of aluminized AHSS', *Math. Model. Weld Phenom 11*, pp. 32s-40s, 2016.

[3] E. GESLAIN: *Soudage par résistance des tôles fines revêtues : formation du noyau dans un assemblage de trois tôles*, thesis, Université de Bretagne Sud, 2018.

[4] R. RAOELISON, A. FUENTES, C. POUVREAU, P. ROGEON, P. CARRE, F. DECHALOTTE : 'Modeling and numerical simulation of the resistance spot welding of zinc coated steel sheets using rounded tip electrode: analysis of required conditions', *Appl. Math. Model 38*, pp. 2505-2521, 2014.

[5] J. WANG, H. P. WANGB, F. LU, B. E. CARLSON, D. R. SIGLER: 'Analysis of Al-steel resistance spot welding process by developing a fully coupled multi-physics simulation model', *International Journal of Heat and Mass Transfer 89*, pp. 1061–1072, 2015.

[6] ZIXUAN WAN, HUI-PING WANG, MIN WANG, BLAIR E. CARLSON, DAVID R. SIGLER, 'Numerical simulation of resistance spot welding of Al to zinc-coated steel with improved representation of contact interactions', *International Journal of Heat and Mass Transfer 101*, pp. 749–763, 2016.

[7] J.M . BERGHEAU: 'Modélisation numérique des procédés de soudage', *Techniques de l'ingénieur*, 2004.

[8] P.S. WEI, S.C. WANG, M.S. LIN, 'Transport phenomena during resistance spot welding', *J. Heat Transfer 118*, pp. 762–773, 1996.

[9] P.S. WEI, T.H. WU : 'Electrical contact resistance effect on resistance spot welding', *International Journal of Heat and Mass Transfer 55*, pp. 3316-3324, 2012.

[10] Y. LI, Z. LUO, Y. BAI, S. S. AO: 'Investigation of induced magnetic force on liquid nugget during resistance spot welding', *Sci. Technol. Weld. Join. 18-4*, pp. 329–336, 2013.

[11] E. GAUTHIER: *Etude expérimentale et numérique de la dégradation cyclique des électrodes en CuCrZr lors du soudage par résistance par point*, thesis, Université de Bretagne Sud, 2014.

[12] G. SIBILIA: *Modélisation du soudage par point : Influence des conditions interfaciales sur le procédé*, thesis, Ecole Polytechnique de l'Université de Nantes, 2003.

[13] G. LE MEUR, G. BOUROUGA AND B. BARDON: 'Microscopic analysis of interfacial electrothermal phenomena – Definition of a heat generation factor', *International Journal of Heat and Mass Transfer 49*, pp. 387-401, 2006.

[14] P. ROGEON, R. N. RAOELISON, P. CARRE AND F. DECHALOTTE: 'A Microscopic Approach to Determine Electrothermal Contact Conditions During Resistance Spot Welding Process', *J. Heat Transfer, vol 131*, pp. 022101-1 – 022101-11, 2009.

[15] S. BABU, M. SANTELLA, Z. FENG, B. RIEMER, J. COHRON, 'Empirical model of effects of pressure and temperature on electrical contact resistance of metals', *Sci. Technol. Weld. Joining 6 (3)*, pp. 126–132, 2001.

[16] E. GESLAIN, P. ROGEON, T. PIERRE, C. POUVREAU AND L. CRETTEUR: 'Coating effects on contact conditions in resistance spot weldability', *Journal of Materials Processing Tech. 253*, pp. 160-167, 2018.